Light-Assisted Resistance Collapse in a V_2O_3-Based Mott-Insulator Device

A. Ronchi,[1,2,3,*] P. Franceschini,[1,2,3] P. Homm,[1] M. Gandolfi,[4,5] G. Ferrini,[2,3] S. Pagliara,[2,3] F. Banfi,[6] M. Menghini,[7,1] J-.P. Locquet,[1] and C. Giannetti[2,3,†]

[1] *Department of Physics and Astronomy, KU Leuven, Celestijnenlaan 200D, Leuven 3001, Belgium*
[2] *Department of Mathematics and Physics, Università Cattolica del Sacro Cuore, Brescia I-25121, Italy*
[3] *ILAMP (Interdisciplinary Laboratories for Advanced Materials Physics), Università Cattolica del Sacro Cuore, Brescia I-25121, Italy*
[4] *CNR-INO, Via Branze 45, Brescia 25123, Italy*
[5] *Department of Information Engineering, University of Brescia, Via Branze 38, Brescia 25123, Italy*
[6] *Université de Lyon, Institut Lumière Matiére (iLM), Université Lyon 1 and CNRS, 10 rue Ada Byron, Villeurbanne Cedex 69622, France*
[7] *IMDEA Nanociencia, Cantoblanco, Madrid 28049, Spain*

(Received 14 October 2020; revised 15 January 2021; accepted 19 March 2021; published 13 April 2021)

The insulator-to-metal transition in Mott insulators is the key mechanism for most of the electronic devices belonging to the Mottronics family. Intense research efforts are currently devoted to the development of specific control protocols, usually based on the application of voltage, strain, pressure, and light excitation. The ultimate goal is to achieve the complete control of the electronic phase transformation, with dramatic impact on the performance, for example, of resistive-switching devices. Here, we investigate the simultaneous effect of external voltage and excitation by ultrashort light pulses on a single Mottronic device based on a V_2O_3 epitaxial thin film. The experiments are supported by both finite-element simulations of the thermal problem and a simpler lumped-element model. The thermal models are benchmarked against results obtained at very low applied voltage ($\Delta V = 5$ mV). When the voltage is significantly increased ($\Delta V = 0.5$ V), but still in the linear below-switching-threshold region, our results show that the light excitation drives a volatile resistivity drop, which goes beyond the combined effect of laser and Joule heating. Our results impact on the development of protocols for the nonthermal control of the resistive-switching transition in correlated materials.

DOI: 10.1103/PhysRevApplied.15.044023

I. INTRODUCTION

Mott insulators are a class of quantum materials exhibiting the most promising properties and functionalities for the next generation of solid-state devices belonging to the Mottronics family [1–4]. Correlated vanadium oxides have been intensively studied due to the possibility of selectively controlling the resistive-switching process at the core of resistive memories and neuromorphic computing [5–8]. The conventional route to control the resistive-switching dynamics is based on the tuning of chemical doping [9–11], temperature [12,13], pressure [14–17], strain [18–20], and on the application of external electric fields [21–25]. More recently, the sudden excitation via ultrashort laser pulses [12,26–33] has been introduced as an additional control parameter, although the nature of the photoinduced insulator-to-metal transition is still subject of intense debate. Much effort has been so far dedicated to the study of the transient optical, electronic, and lattice properties [12,26–33] and on the role of intrinsic nanoscale inhomogeneities [12,13,34] with the goal of understanding to what extent the photoinduced transition is similar to the thermally driven one. In contrast, little is known about the actual resistive state that is induced by light excitation possibly combined with external voltage. Recent theoretical works have suggested that, in the vicinity of the insulator-metal coexisting region, the application of voltage [23] and the excitation with light pulses capable of manipulating the band occupation [12,35], can lead to the weakening of the insulating state and, eventually, to the complete collapse of the Mott insulating phase and the consequent resistive switching along a nonthermal pathway.

Here we develop a Mottronic device, based on a microbridged V_2O_3 epitaxial thin film, in which the resistance state consequent to a controlled excitation by trains of ultrashort light pulses can be measured. V_2O_3 is a prototypical Mott insulator that exhibits a first-order insulator-to-metal transition (IMT) occurring at $T_{IMT} \sim 170$ K and characterized by a resistivity change of several

*andrea.ronchi@unicatt.it
†claudio.giannetti@unicatt.it

orders of magnitude [14,15,17]. When a voltage larger than a temperature-dependent threshold $\Delta V_{\rm th}$ is applied in the insulating state ($T < T_{\rm IMT}$), the device undergoes a resistive-switching process, i.e., the resistance suddenly drops to the metallic value. However, the switching process in V_2O_3 devices is associated to the formation of micrometric conductive filaments [25], which usually makes the evaluation of the local heating and the investigation of the thermal nature of the dynamics rather difficult. In order to avoid this additional complexity, we investigate the light-induced volatile resistance drop for different applied voltages, always smaller than $\Delta V_{\rm th}$. We work in the reversible regime, in which the voltage-current curve does not present any discontinuity suggesting the formation of below-threshold filaments [25]. The light-induced below-threshold resistance drop thus provides information about the weakening of the insulating phase, triggered by the combined voltage-light excitation, while avoiding the formation of the conductive channels associated to the resistive-switching process. Starting from the resistance versus temperature calibration curve of the device, we are able to compare the photoinduced resistivity drop to the local heating effect, which is carefully estimated by both finite-element simulations and a more intuitive lumped-element model. Our main results can be summarized as follows. For low applied voltage ($\Delta V = 5$ mV), the application of a sufficiently long train of light pulses drives a volatile resistance drop that is fully compatible with that predicted by finite-element simulations of the thermal problem. This thermal case thus acts as the actual calibration of the system and ensures that both the incident heating power and the dissipations are correctly accounted for. The minimum number of pulses necessary to observe a significant effect suggests that the light-induced local heating is mediated by the electronic specific heat, which becomes extremely large as $T_{\rm IMT}$ is approached. In contrast to the previous low-voltage case, when a significant below-threshold electrical bias ($\Delta V = 0.5$ V) is applied, the light-induced volatile drop of the resistance is twice what is expected by considering both the laser-induced and Joule heating. This result leads to the conclusion that the combined voltage-light excitation protocol makes the system more fragile towards the collapse of the insulating electronic phase.

II. METHODS

A. Mottronic device

An epitaxial V_2O_3 film with thickness $d = 67$ nm is deposited by oxygen-assisted molecular beam epitaxy (MBE) in a vacuum chamber with a base pressure of 10^{-9} Torr. A 37-nm Cr_2O_3 buffer layer is interposed between the film and the substrate to minimize lattice mismatch and optimize strain relaxation in the film. A (0001)-Al_2O_3 substrate is used without prior cleaning and is slowly heated to a growth temperature of 700 °C. Vanadium is evaporated from an electron gun with a deposition rate of 0.1 Ås^{-1}, and an oxygen partial pressure of 6.2×10^{-6} Torr is used during the growth [18]. Under these conditions, a single-crystal film with the c axis oriented perpendicular to the surface is obtained. A microbridge, constituted by 40-nm-Au/5-nm-Ti-thick electrodes with $w = 50$ μm width and $s = 2$ μm separation, is nanopatterned on the film surface, as shown in Fig. 1(a). Temperature-dependent resistivity measurements [see Fig. 1(b)] are performed using a Keithley Sourcemeter 2634B in the two-point configuration across the Au/Ti electrodes. The device temperature is controlled by a closed cycle cryostat equipped with a heater. The temperature sweep rate is set to 0.5 K per minute. When cooled down, the device undergoes the metal-to-insulator transition, characterized by a resistance increase of almost 3 orders of magnitude. In our device the resistance ranges from 20 Ω at room temperature (metallic state) to 130 kΩ at $T = 140$ K (insulating state). The heating and cooling branches evidence the typical hysteresis cycle of the IMT, which spans the insulator-metal coexistence region from 155 to 185 K. In the following, we consider $T_{\rm IMT} \simeq 170$ K as the temperature corresponding to the midpoint of the heating branch of the hysteresis cycle. Within the coexistence region and at fixed temperature, the application of a large enough voltage across the device can induce the resistive switching. In the panel of Fig. 1(b) we show the voltage-current curve of the device at $T = 160$ K. The voltage threshold necessary to obtain the resistive switching at this temperature is $\Delta V_{\rm th} \simeq 2.5$ V. Below this threshold, the voltage-current curve is fully reversible and does not show any discontinuity related to the possible formation of subthreshold metallic filaments.

B. Photoinduced resistance drop measurements

Resistance measurements are combined with light excitation by focusing a train of infrared pulses (0.4 μJ, 50 fs) at 800-nm wavelength (1.55-eV photon energy) generated by an optical parametric amplifier pumped by an Yb-laser system. A pulse picker allows both the repetition rate, set to 25 kHz, and the total number of pulses impinging on the sample to be controlled. The laser output is focused on the device by a 10-cm lens. The FWHM of the spot size on the device is 50 μm, as measured using the knife-edge technique. The pump incident fluence on the device is of the order of 0.2 mJ/cm^2, which is below the threshold necessary to photoinduce the complete insulator-to-metal transition [12]. In Fig. 1(c) we show the typical resistance drop measured after excitation with a controlled number of light pulses (200 kpulses at 25-kHz repetition rate). Prior to the experiment the device is cooled down to 100 K and then heated up to $T \simeq 160$ K, i.e., in the insulator-metal coexistence region. Before light excitation, the system is thus in a high resistivity state along the heating branch

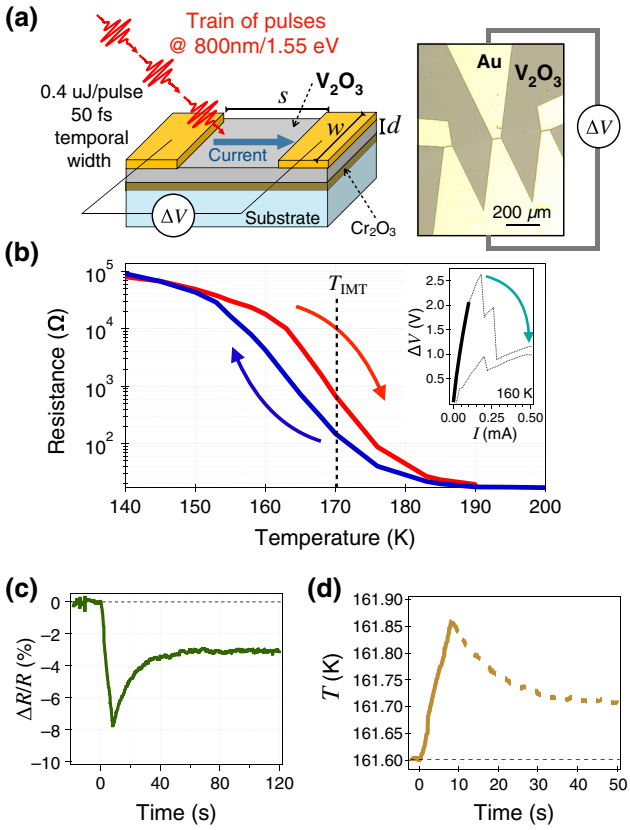

FIG. 1. Working principle of the experiment. (a) Left: sketch of the experimental setup. A finite train of laser pulses ($\hbar\omega =$ 1.55 eV, 50-fs temporal width, $\nu = 25$ kHz) is used to photoexcite the device. The change in the two-point resistance of the device is simultaneously measured before, during, and after the laser excitation by means of Au/Ti electrodes. The contact resistance can be neglected since is very small (approximately 5 Ω) with respect to the V_2O_3 bridge resistance (approximately 15 kΩ). Right: microscopic image of the device used during the experiment. (b) Equilibrium two-point resistance hysteresis measured as a function of the temperature. The red (blue) arrows indicate the heating (cooling) branch. Inset: two-point I-V curve showing volatile resistive switching at $T = 160$ K. The black thicker line highlights the below-threshold region in which the I-V curve is fully reversible. The measurement is performed through the 2-μm gap shown in (a). (c) Relative variation of resistance measured across the device as a function of the time delay at the base temperature $T_0 = 161.6$ K. The time zero corresponds to the moment when the first pulse of the laser train arrives. (d) Result of the conversion of resistance drop measurements [see (c)] into effective local temperature (yellow solid line). The resistance versus temperature curve shown in Fig. 1(b) is inverted to obtain, for each value of resistance, the corresponding local temperature. As explained in the main text, the cooling down process takes place along a resistance-temperature curve, which differs from the equilibrium one reported in (b). The dashed line, corresponding to the cooling-down dynamics of the system, is the hypothetical local temperature obtained from the heating branch of the equilibrium resistance-temperature curve, but does not necessarily represent the actual local effective temperature of the system.

of the hysteresis curve shown in Fig. 1(b). Laser excitation is then switched on and the time-dependent resistance is obtained by measuring the current flowing across the bridge at a fixed applied voltage ($\Delta V = 5$ mV) and at the nominal temperature $T = 160$ K. After 8 s, i.e., at the end of the pulse train, the resistance drops by 8% with respect to the initial value. Once the light excitation is removed, the relative resistance variation, i.e., $\Delta R/R$, starts to decrease, until it reaches a plateau corresponding to a nonvolatile change of about 3%. The explanation of this effect resides in the inherent hysteresis of the IMT [see Fig. 1(b)]: after the laser-induced warming up, which is not enough to drive the system out of the hysteresis region, the cooling down takes place along a curve located somewhere between the complete warming-up and cooling-down curves [red and blue curves in Fig. 1(b)]. The final resistance value is therefore smaller than the initial value, although the initial temperature is recovered. In order to restore the initial resistance value, the device must undergo a complete thermal cycle, corresponding to heating up to 300 K, followed by cooling down to 100 K, and further heating up to $T \simeq 160$ K. The same thermal cycle protocol is applied before any of the resistance-drop measurements reported in the following.

The resistance-temperature curve shown in Fig. 1(b) can be used to retrieve the precise local effective temperature of the V_2O_3 device during the light-excitation process, as shown in Fig. 1(d). The local effective temperature during the resistance drop is extracted by interpolating and inverting the heating branch of the resistance-temperature curve [Fig. 1(b)]. The error associated to the local effective temperature is obtained by considering the accuracy of the Keithley Sourcemeter (±0.02 %) in the voltage range used during the experiments. We stress that the resistance-temperature relation is single-valued only along the heating branch. Therefore, the resistance value can be converted in the actual local temperature only during the heating-up process in the 0–8 s time span. During the cooling down (8–120 ps) the resistance moves back along a nonequilibrium resistance-temperature curve, which differs from that used for calibration [Fig. 1(b)] and cannot therefore be used to retrieve the actual local temperature.

C. Finite-element-method simulation of the thermal problem

The heating induced by the laser excitation is numerically simulated by finite-element methods (COMSOL Multiphysics). In the simulations we consider the 67-nm-thick V_2O_3 film on top of a 500-μm-thick (0001)-Al_2O_3 substrate. The Cr_2O_3 buffer layer is omitted since its thermal and optical properties are very similar to the sapphire's ones. The problem is solved in two-dimensional (2D) axial symmetry in a region with 800-μm diameter. A representation of the sample cross section is reported in the inset

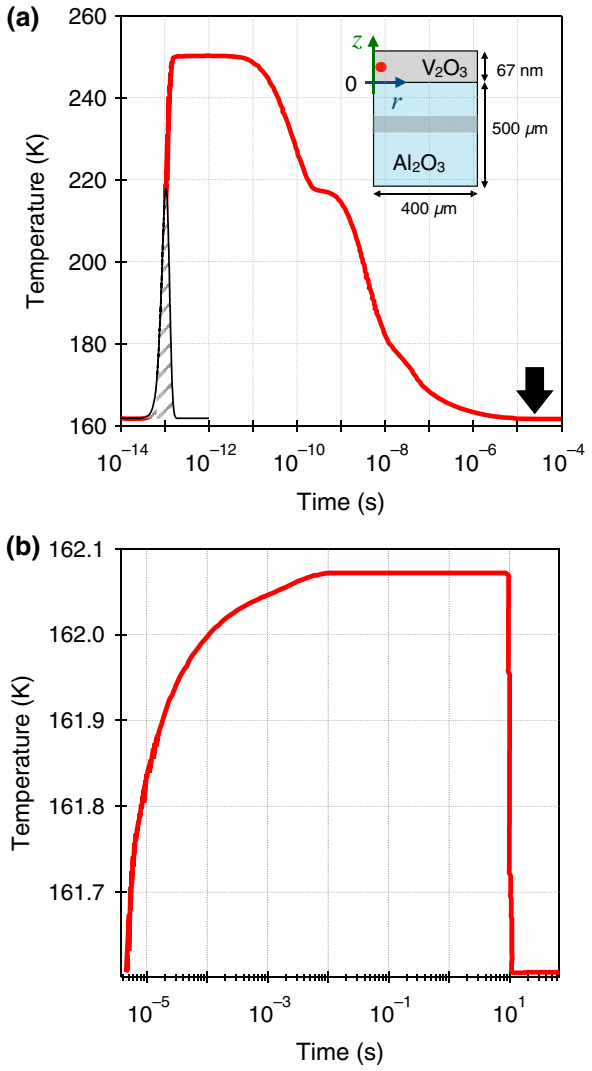

FIG. 2. Finite-element-method simulations. (a) The solid line represents the temperature increase due to the single-pulse excitation (black dashed area) as a function of the time (logarithmic scale). The black arrow indicates the instant ($t = 40$ μs) at which the following pulse arrives. Inset: sketch of the geometry used in the COMSOL simulations. The red dot indicates the point at which the temperature is evaluated ($r = 50$ nm; $z = 33.5$ nm). (b) The temperature variation at saturation, induced by 2×10^5 laser pulses, is shown. The temperature is evaluated at half of the total thickness, i.e., $r = 50$ nm and $z = 33.5$ nm. The maximum temperature reached after the excitation with the pulse train is used as the input to build the curves reported in Fig. 3.

of Fig. 2(a). Thermal insulating boundary conditions are applied on the top and lateral boundaries, whereas the sapphire bottom boundary ($z = -500$ μm) is kept at the constant temperature $T_0 = 161.6$ K, which corresponds to the actual initial effective temperature of the device, as extracted from the resistance value.

The thermal problem for single-pulse excitation is initially addressed. In this configuration, a single pulse with temporal and spatial Gaussian profiles matching the experimental ones, excites the sample. We consider an energy density delivered to the system (0.66 kJ/cm^3) such that the time and spatial integral matches the total energy released by the laser pulse upon accounting for reflection losses. The estimated energy absorbed within the 67-nm V_2O_3 film is calculated with a multireflection model (total absorption $A = 0.22$), assuming the optical constants reported in the literature [36]. Using Fourier's law, the energy balance within the volume of the V_2O_3 film reads

$$-\nabla \cdot \left\{ -\kappa[T(r,z,t)]\nabla T(r,z,t) \right\} + P(r,z,t) = \rho\, c_p[T(r,z,t)] \frac{\partial T(r,z,t)}{\partial t}, \quad (1)$$

where $P(r,z,t)$ is the absorbed pulsed power-density profile, $\kappa(T)$ is the temperature-dependent thermal conductivity [37], ρ the mass density, and $c_p(T)$ the temperature-dependent total specific heat at constant pressure [38]. For sake of completeness, the parameters used in the simulation are reported in Table I. The following heat-flux continuity boundary condition is used at the V_2O_3/Al_2O_3 interface:

$$k_{V_2O_3} \left.\frac{\partial T}{\partial z}\right|_{z=0^+} = k_{Al_2O_3} \left.\frac{\partial T}{\partial z}\right|_{z=0^-}. \quad (2)$$

The initial condition is $T_0 = 161.6$ K throughout the sample and the substrate. The equation is solved via the finite-element method, covering a time scale spanning 7 orders of magnitude. Since the presence of a thermal boundary resistance (TBR) at the V_2O_3/Al_2O_3 interface can affect the temperature of the V_2O_3 film, simulations with different TBR values are performed. Assuming a TBR (10^{-7} m^{2}KW^{-1}) 1 order of magnitude larger than typical values reported for similar materials [42], leads to a correction of the V_2O_3 temperature profile smaller than 10%, i.e., within the experimental uncertainty. The thermal dynamics of the single-pulse excitation is shown in Fig. 2(a). We remark that we are interested in thermal dynamics on time scales longer than the pulse duration and the typical time of electron-phonon coupling. Therefore, we assume the complete thermalization between the electron and lattice subsystems, as implied by the use of the total specific heat and thermal conductivity values.

After the impulsive energy absorption, the temperature reaches its maximum value (approximately 250 K) within few picoseconds. Subsequently, the energy diffusion through the sapphire substrate drives the slower cooling-down process. If we consider the time needed to reduce the initial temperature variation by a factor 2, we obtain a half-life of about 2 ns. The cooling down to the initial temperature $T_0 = 161.6$ K is almost completed within approximately 40 μs, although a small temperature

TABLE I. Summary of the material parameter values adopted in the present work for finite-element-method simulations.

Parameter	Value	Units	Ref.
$c_p(T)\big\|_{V_2O_3}$	$c_p(T = 160\ \mathrm{K}) = 480$	J kg^{-1} K^{-1}	[38]
	$c_p(T_{\mathrm{IMT}}) = 2400$	J kg^{-1} K^{-1}	[38]
	$c_p(T = 190\ \mathrm{K}) = 530$	J kg^{-1} K^{-1}	[38]
$c_p\big\|_{Al_2O_3}$	776	J kg^{-1} K^{-1}	[39]
$\kappa(T)\big\|_{V_2O_3}$	$\kappa(T)$ (approximately 3.1 @160 K)	W m^{-1} K^{-1}	[37]
$\kappa\big\|_{Al_2O_3}$	35	W m^{-1} K^{-1}	[40]
$\rho_{V_2O_3}$	4870	kg m^{-3}	[39]
$\rho_{Al_2O_3}$	3980	kg m^{-3}	[39]
$\mathrm{Re}(\tilde{n}_{V_2O_3})$	1.997 @800 nm	kg m^{-3}	[36]
$\mathrm{Im}(\tilde{n}_{V_2O_3})$	0.382 @800 nm	kg m^{-3}	[36]
$\mathrm{Re}(\tilde{n}_{Al_2O_3})$	1.76 @800 nm	kg m^{-3}	[41]

increase approximately 0.04 K persists. The simulations also demonstrate that, in the device region, the temperature variation within the V_2O_3 film is rather homogeneous, with less than 1% difference between the top and bottom temperatures. For the sake of simplicity, in the following we refer to the temperature of the point at 33.5-nm distance from the device surface [see Fig. 2(a)].

In the multipulse experimental configuration, the heating associated to each pulse accumulates on top of the temperature increase triggered by the previous ones. Considering a pulse distance of 40 μs (25-kHz repetition rate), the small temperature difference accumulated after each pulse leads to a progressive increase of the local effective temperature, until the external heat flux is balanced by the dissipation. In this condition, the average effective temperature does not further increase and it reaches a saturation value, which ultimately drives the resistance drop across the bridge observed after the light excitation. For simplicity, the effect of the total thermal heating induced by the multipulse excitation is simulated by considering a laser beam with steplike temporal profile extending over the same time span of the pulse train and with the same average power [40,43,44]. An example of the temperature dynamics, for a train of 2×10^5 pulses, is shown in Fig. 2(b). The heat accumulation leads, at saturation, to a final temperature of 162.1 K. The discrepancy between this value and the experimental one [see Fig. 2(b)] will be clarified in the next section. Once the input power is removed, the system rapidly cools down to the initial temperature. For a better comparison with the experimental data, the time-dependent temperature curves obtained by the simulations and reported in Fig. 2(b) are subsequently filtered by a low-pass filter with a bandwidth corresponding to the cutoff frequency (10 Hz) of the electrical circuit used for the resistance measurements.

III. RESULTS AND DISCUSSION

A. Calibration of the thermal model

As a first step, we benchmark the thermal model against the experimental results obtained when the applied voltage across the device is $\Delta V = 5$ mV, i.e., much smaller than the threshold $\Delta V_{\mathrm{th}} \simeq 2.5$ V necessary to obtain the resistive switching at the working temperature $T = 160$ K. In Fig. 3(a) the experimental points (green circles) represent the maximum laser-induced effective temperature increase, estimated by the volatile resistance drop described in Sec. II B, as a function of the number of excitation pulses. We stress that each experimental point is obtained after a complete thermal cycle, necessary to restore the initial resistance of the device (see Sec. II A). The data show that no significant temperature increase is detectable below approximately 10^4 pulses. Above this threshold the temperature increases and saturates after approximately 10^6 pulses. The temperature achieved in the saturation regime, i.e., when the excitation average power matches the thermal losses towards the substrate, is approximately 162.06 K.

In order to rationalize the laser-induced dynamics of the temperature $T(t)$ and address the strengths and limits of the full thermal numerical model, we introduce here a simpler yet analytic lumped-element model of the kind commonly adopted to rationalize transient heat transfer in time-resolved experiment [40]:

$$C_t \frac{d(T - T_0)}{dt} = W - \frac{1}{R_{\mathrm{th}}}(T - T_0), \tag{3}$$

where $T_0 = 161.6$ K is the initial temperature, C_t represents the total heat capacity of the device, W is the total absorbed power, R_{th} is a constant with the dimensions of a thermal resistance and effectively accounts for the total heat dissipation. Independently of the specific values of the effective coefficients entering in the lumped-element model, the general solution of Eq. (3) is the exponential function $T(t) = T_0 + \delta T_{\mathrm{sat}}(1 - e^{-t/\tau})$, where $\tau = R_{\mathrm{th}} C_t$ is the time constant of the heating-up process and $\delta T_{\mathrm{sat}} = R_{\mathrm{th}} W$ is the temperature variation at saturation. This exponential function can be used to fit the data and retrieve the experimental time constant of the system. The red solid line in Fig. 3(a) is the exponential fit, which provides $\tau = 18.5 \pm 0.8$ s corresponding to $(4.6 \pm 0.2) \times 10^5$ pulses. We stress here that the saturation temperature increase, δT_{sat}, is only controlled by the input power and the total dissipation, whereas the heating time constant depends on the heat capacity of the system.

The local effective temperature retrieved by the resistance drop is compared to the results of calculations of the full thermal problem, as described in Sec. II C. The black solid line in Fig. 3(a) represents the saturation temperature increase obtained by finite-element calculations, when

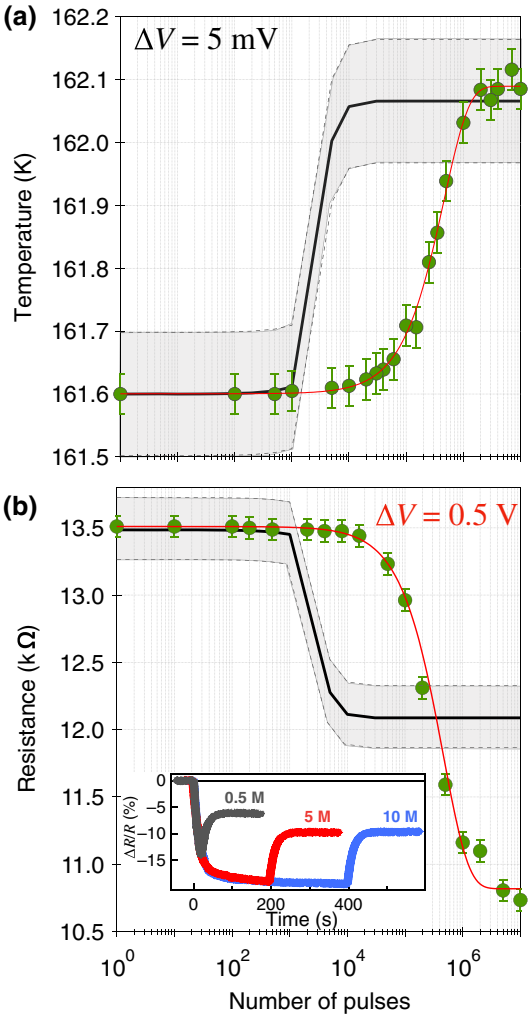

FIG. 3. Comparison between experimental and numerical results. (a) Maximum variation of the sample's temperature induced by the laser pulses as a function of the total number of pulses (green circles). The applied voltage is $\Delta V = 5$ mV. The solid black line represents the simulated data where the maximum temperature is extracted for each finite number of pulses. The gray area shows the error interval associated to the model assumptions and numerical approximations. The red solid line represents the exponential fit to the experimental data. (b) Maximum laser-induced drop of the device resistance when a constant voltage bias $\Delta V = 0.5$ V is applied across the Au/Ti electrodes (green circles). The solid black line represents the outcome of numerical simulations, from which the expected resistance drop is retrieved from the local effective heating for each finite number of pulses. The dissipated power related to the Joule heating has been added to the power dissipated by the laser excitation. The gray areas show the error interval associated to the model assumptions and numerical approximations. The solid red line represents the exponential fit to the experimental data. In the inset we report the time-dependent relative resistance variation curves measured with $\Delta V = 0.5$ V applied voltage for different numbers of excitation pulses (gray, 0.5×10^6 pulses; red, 5×10^6 pulses; blue, 10×10^6 pulses). The maximum resistance variation for each curve is reported as a single data point in the main panel.

an average power corresponding to that of the pulse train exciting the device is considered. The calculated saturation temperature increase, i.e., $\delta T_{\mathrm{sat}} = 0.5$ K perfectly matches the experimental value. Considering that δT_{sat} depends only on the adsorbed power W and on R_{th}, we thus can conclude that the finite-element calculations perfectly account for both the heating power and the total dissipation, which is ultimately regulated by the heat diffusion throughout the V_2O_3 film and the substrate.

The difference between the calculated and measured time constants of the exponential heating dynamics can be attributed to an underestimation of the total heat capacity C_t. Throughout the calculations of the thermal problem, we assume perfect electron-phonon thermalization and we thus consider the V_2O_3 temperature-dependent total specific heat [38]. Nonetheless, the absorption of each single light pulse is mediated by the electronic population which undergoes a large temperature increase. The effective electronic temperature dynamically overcomes the Mott insulator-to-metal transition temperature T_{IMT}, which is accompanied by a divergence of the electronic effective mass m^*. Considering that the electronic specific heat of an electron gas $c_{\mathrm{el}} \propto m^{*3/2}$, the dynamical crossing of T_{IMT} is naturally accompanied by a large increase of c_{el} [38], which is characterized by a narrow cusp centered at T_{IMT} (see Table I). In the vicinity of the Mott transition, the electron gas thus behaves like a reservoir capable of absorbing a large quantity of energy but limiting the impulsive increase of the effective temperature of the electron-phonon system. Our experimental results are compatible with $c_{\mathrm{el}} = (30 \pm 6) \times c_p(T_{\mathrm{IMT}})\big|_{V_2O_3}$, which suggests an effective mass increase of 10, compatible with what recently observed in VO_2 [45] and attributed to the strong electronic correlations.

B. Nonthermal below-threshold resistance collapse

In the previous section we assess the validity of the thermal model in accounting for the absorbed power and the heat dissipation and in correctly predicting the laser-induced heating in the saturation regime. In this section we compare the expected thermally induced resistance drop to what is actually measured when the laser pulses are combined to a voltage that is no longer negligible with respect to ΔV_{th}. We stress that the light-excitation protocol is exactly the same as the low-voltage case discussed before. In Fig. 3(b) we report the resistance drop, measured following the procedure previously described, with $\Delta V = 0.5$ V applied voltage. In this case, although the resistance drop is described by an exponential function (solid red line) with the same time constant ($\tau = 18.7 \pm 1.6$ s), the value achieved in the saturation regime ($\delta R_{\mathrm{sat}} \simeq 2.6$ kΩ) is twice the value measured ($\delta R_{\mathrm{sat}} \simeq 1.3$ kΩ) for $\Delta V = 5$ mV. For the sake of clarity, in the inset of Fig. 3(b) we report some of the full individual experimental traces representing the

time-dependent resistance drop during and after the application of a large number of pulses. When the number of pulses exceeds approximately 5×10^5 the time-dependent traces saturate to the $\delta R_{\rm sat}$ value.

The resistance drop measured under the applied bias $\Delta V = 0.5$ V is compared to the value expected by considering the laser-induced heating (the parameters of the thermal calculations are the same as the previous low-voltage case) and also including the effect of Joule heating induced by the current flowing throughout the V_2O_3 bridge. We stress that the voltage applied through the device is smaller than the threshold value necessary for the resistive switching. Therefore, in this regime no metallic filaments [25], possibly responsible for large local Joule heating, are created and the system can be treated as homogeneous. The additional dissipated power can be thus written as

$$\Delta P_J = \frac{\Delta V \times I}{s \times w \times d}, \tag{4}$$

where ΔP_J is the power density dissipated by the electrical current I flowing through the electrodes and $s \times w \times d$ is the device effective volume [see Fig. 1(a)]. ΔP_J is added to the total power density $P(r,z)$, provided by the pulse train, in Eq (1). The black solid line in Fig. 3(b) represents the result of the numerical simulation converted in the expected resistance drop by means of the resistance versus temperature calibration curve [see Fig. 1(b)]. We note that the Joule heating induced by the current is of the order of 2×10^{-5} W and is negligible as compared to the laser power, which amounts to approximately 10^{-2} W. As a conclusion, the additional Joule heating does not account for the measured resistivity drop in the stationary regime, which is twice that expected from heating alone.

The present results can be rationalized on the basis of recent theoretical work [23], which showed that in the insulator-metal coexistence region, the application of a significant electric field is able to induce the nonthermal weakening of the Mott insulating phase via the formation of metallic states at the Fermi level with no counterpart at equilibrium. This mechanism is in sharp contrast with the conventional Zener tunneling mechanism that is usually invoked to describe the resistive-switching dynamics. Interestingly, the state variable that characterizes the transition and controls the free energy of the system is the orbital polarization, defined as $p = n_{e_g^\pi} - n_{a_{1g}}$, where $n_{e_g^\pi}$ is the occupation of the lowest energy V-3d e_g^π orbitals and $n_{a_{1g}}$ is the occupation of the V-3d a_{1g} orbitals. The Mott insulating phase is characterized by $p = 2$, whereas the application of an electric field induces the formation of a metallic state with $p = 1.2 - 1.6$ [23]. As recently shown [12], the excitation with infrared light pulses with 1.55-eV photon energy can induce a further orbital polarization decrease of the order of $\delta p \simeq -10^{-3} - 10^{-2}$, which in turn leads to a change of 1.3–13 meV of the difference between the free energies of the insulating and metallic phases. The photoinduced change of the free-energy difference largely overcomes the thermal effect, i.e., $k_B \delta T \simeq 50$ μeV, thus inducing the growth of already existing metallic domains in the insulator-metal coexistence region. The combination of below-threshold voltage and the excitation with infrared light pulses capable of modifying the occupation of vanadium orbitals thus weakens the insulating state well beyond what can be ascribed to thermal effects. The scenario emerging from our results can be understood also within the resistor network model [21], which is commonly adopted to describe the insulator-to-metal switching dynamics. In this model, the physical system is divided in nanometric cells representing small regions, which are either in the insulating (high-resistance) or metallic (low-resistance) states. The combined action of voltage and laser excitation leads to a nonthermal increase of the number of the metallic cells, thus triggering the observed volatile resistance drop. Working with below-threshold voltage and with weak laser excitation avoids the creation of connected filamentary metallic paths, which are responsible for the resistive-switching process observed above $\Delta V_{\rm th}$.

IV. CONCLUSIONS

In conclusion, we investigate the simultaneous action of a train of infrared light pulses and an external voltage on a Mottronic device based on V_2O_3, which undergoes an IMT at $T_{\rm IMT} \simeq 170$ K. When the device is in the insulator-metal coexisting region ($T \simeq 160$ K) and a 0.5-V voltage is applied across the device, the measured resistance drop induced by a pulse number exceeding 10^6 is twice that expected from the simple local heating of the device. Our results suggest that although the 0.5-V applied voltage is below the threshold ($\Delta V_{\rm th} = 2.5$ V) necessary for inducing the complete and irreversible resistive switch, it brings the insulating phase close to the insulator-to-metal instability. The simultaneous weak excitation with a sufficient number of infrared pulses modifies the occupation of the vanadium 3d orbitals enough to trigger the nonthermal growth and proliferation of already existing metallic nodes, well beyond what can be ascribed to the total local heating induced by the laser-voltage combination. The present results also call for the development of time-resolved microscopy techniques to investigate the real time dynamics of the metallicity in Mottronics and resistive-switching devices subject to the simultaneous application of electric fields and light pulses.

ACKNOWLEDGMENTS

C.G., A.R., and P.F. acknowledge Andrea Tognazzi for the support in the development of the experimental setup. C.G. and A.R. acknowledge Dr. Alessandro Bau' and Professor Vittorio Ferrari (Information Engeenering Department, Università degli Studi di Brescia) for the

support given during the wirebonding of the device. We thank Frederik Ceyssens for his help with the fabrication of electrical contacts on the samples. C.G., A.R., and P.F. acknowledge financial support from MIUR through the PRIN 2017 program (Prot. 20172H2SC4_005). G.F. and C.G. acknowledge support from Università Cattolica del Sacro Cuore through D.1, D.2.2, and D.3.1 Grants. F.B. acknowledges financial support from Université de Lyon in the frame of the IDEXLYON Project-Programme Investissements d'Avenir (ANR-16-IDEX-0005) and from Université Claude Bernard Lyon 1 thorugh the BQR Accueil EC 2019 Grant. P.H., M.M., and J.-P.L. acknowledge support from EU-H2020-ICT-2015 PHRESCO Project, Grant Agreement No. 688579. P.H. acknowledges support from Becas Chile-CONICYT. M.G. acknowledges financial support from the CNR Joint Laboratories program 2019-2021.

[1] Y. Tokura, M. Kawasaki, and N. Nagaosa, Emergent functions of quantum materials, Nat. Phys. **13**, 1056 (2017).

[2] Z. Yang, C. Ko, and S. Ramanathan, Oxide electronics utilizing ultrafast metal-insulator transitions, Annu. Rev. Mater. Res. **41**, 337 (2011).

[3] J. Zhang and R. D. Averitt, Dynamics and control in complex transition metal oxides, Annu. Rev. Mater. Res. **44**, 19 (2014).

[4] D. N. Basov, R. D. Averitt, and D. Hsieh, Towards properties on demand in quantum materials, Nat. Mater. **16**, 1077 (2017).

[5] Y. Zhou and S. Ramanathan, Mott memory and neuromorphic devices, Proc. IEEE **103**, 1289 (2015).

[6] E. Janod, J. Tranchant, B. Corraze, M. Querré, P. Stoliar, M. Rozenberg, T. Cren, D. Roditchev, V. T. Phuoc, M.-P. Besland, and L. Cario, Resistive switching in Mott insulators and correlated systems, Adv. Funct. Mater. **25**, 6287 (2015).

[7] J. del Valle, J. G. Ramírez, M. J. Rozenberg, and I. K. Schuller, Challenges in materials and devices for resistive-switching-based neuromorphic computing, J. Appl. Phys. **124**, 211101 (2018).

[8] P. Salev, J. del Valle, Y. Kalcheim, and I. K. Schuller, Giant nonvolatile resistive switching in a Mott oxide and ferroelectric hybrid, Proc. Natl. Acad. Sci. **116**, 8798 (2019).

[9] H. Kuwamoto, J. M. Honig, and J. Appel, Electrical properties of the $(V_{1-x}Cr_x)_2O_3$ system, Phys. Rev. B **22**, 2626 (1980).

[10] P. Homm, L. Dillemans, M. Menghini, B. Van Bilzen, P. Bakalov, C.-Y. Su, R. Lieten, M. Houssa, D. Nasr Esfahani, L. Covaci, F. M. Peeters, J. W. Seo, and J.-P. Locquet, Collapse of the low temperature insulating state in Cr-doped V_2O_3 thin films, Appl. Phys. Lett. **107**, 111904 (2015).

[11] J. del Valle, Y. Kalcheim, J. Trastoy, A. Charnukha, D. N. Basov, and I. K. Schuller, Electrically Induced Multiple Metal-Insulator Transitions in Oxide Nanodevices, Phys. Rev. Appl. **8**, 054041 (2017).

[12] A. Ronchi, P. Homm, M. Menghini, P. Franceschini, F. Maccherozzi, F. Banfi, G. Ferrini, F. Cilento, F. Parmigiani, S. S. Dhesi, M. Fabrizio, J.-P. Locquet, and C. Giannetti, Early-stage dynamics of metallic droplets embedded in the nanotextured Mott insulating phase of V_2O_3, Phys. Rev. B **100**, 075111 (2019).

[13] A. S. McLeod, E. van Heumen, J. G. Ramírez, S. Wang, T. Saerbeck, S. Guenon, M. Goldflam, L. Anderegg, P. Kelly, A. Mueller, M. K. Liu, Ivan K. Schuller, and D. N. Basov, Nanotextured phase coexistence in the correlated insulator V_2O_3, Nat. Phys. **13**, 80 (2016).

[14] D. B. McWhan, T. M. Rice, and J. P. Remeika, Mott Transition in Cr-Doped V_2O_3, Phys. Rev. Lett. **23**, 1384 (1969).

[15] A. Jayaraman, D. B. McWhan, J. P. Remeika, and P. D. Dernier, Critical Behavior of the Mott Transition in Cr-Doped V_2O_3, Phys. Rev. B **2**, 3751 (1970).

[16] I. Valmianski, Juan Gabriel Ramirez, C. Urban, X. Batlle, and Ivan K. Schuller, Deviation from bulk in the pressure-temperature phase diagram of V_2O_3 thin films, Phys. Rev. B **95**, 155132 (2017).

[17] P. Limelette, A. Georges, D. Jérome, P. Wzietek, P. Metcalf, and J. M. Honig, Universality and critical behavior at the Mott transition, Science **302**, 89 (2003).

[18] L. Dillemans, T. Smets, R. R. Lieten, M. Menghini, C.-Y. Su, and J.-P. Locquet, Evidence of the metal-insulator transition in ultrathin unstrained V_2O_3 thin films, Appl. Phys. Lett. **104**, 071902 (2014).

[19] D. Lee *et al.*, Isostructural metal-insulator transition in VO_2, Science **362**, 1037 (2018).

[20] Y. Kalcheim, N. Butakov, N. M. Vargas, M.-H. Lee, J. del Valle, J. Trastoy, P. Salev, J. Schuller, and I. K. Schuller, Robust Coupling between Structural and Electronic Transitions in a Mott Material, Phys. Rev. Lett. **122**, 057601 (2019).

[21] P. Stoliar, L. Cario, E. Janod, B. Corraze, C. Guillot-Deudon, S. Salmon-Bourmand, V. Guiot, J. Tranchant, and M. Rozenberg, Universal electric-field-driven resistive transition in narrow-gap mott insulators, Adv. Mater. **25**, 3222 (2013).

[22] S. Guénon, S. Scharinger, Siming Wang, J. G. Ramírez, D. Koelle, R. Kleiner, and Ivan K. Schuller, Electrical breakdown in a V_2O_3 device at the insulator-to-metal transition, EPL (Europhysics Letters) **101**, 57003 (2013).

[23] G. Mazza, A. Amaricci, M. Capone, and M. Fabrizio, Field-Driven Mott Gap Collapse and Resistive Switch in Correlated Insulators, Phys. Rev. Lett. **117**, 176401 (2016).

[24] J. del Valle, P. Salev, F. Tesler, N. M Vargas, Y. Kalcheim, P. Wang, J. Trastoy, M.-H. Lee, G. Kassabian, J. G. Ramírez, M. J. Rozenberg, and I. K. Schuller, Subthreshold firing in mott nanodevices, Nature **569**, 388 (2019).

[25] Y. Kalcheim, A. Camjayi, J. del Valle, P. Salev, M. Rozenberg, and I. K. Schuller, Non-thermal resistive switching in Mott insulator nanowires, Nat. Commun. **11**, 2985 (2020).

[26] B. Mansart, D. Boschetto, S. Sauvage, A. Rousse, and M. Marsi, Mott transition in Cr-doped V_2O_3 studied by ultrafast reflectivity: Electron correlation effects on the transient response, EPL (Europhysics Letters) **92**, 37007 (2010).

[27] M. K. Liu, B. Pardo, J. Zhang, M. M. Qazilbash, Sun Jin Yun, Z. Fei, Jun-Hwan Shin, Hyun-Tak Kim, D. N. Basov,

and R. D. Averitt, Photoinduced Phase Transitions by Time-Resolved Far-Infrared Spectroscopy in V_2O_3, Phys. Rev. Lett. **107**, 066403 (2011).

[28] E. Abreu, S. Wang, J. G. Ramírez, M. Liu, J. Zhang, K. Geng, I. K. Schuller, and R. D. Averitt, Dynamic conductivity scaling in photoexcited V_2O_3 thin films, Phys. Rev. B **92**, 085130 (2015).

[29] V. R. Morrison, R. P. Chatelain, K. L. Tiwari, A. Hendaoui, A. Bruhács, M. Chaker, and B. J. Siwick, A photoinduced metal-like phase of monoclinic VO_2 revealed by ultrafast electron diffraction, Science **346**, 445 (2014).

[30] E. Abreu, S. N. Gilbert Corder, S. J. Yun, S. Wang, J. G. Ramírez, K. West, J. Zhang, S. Kittiwatanakul, I. K. Schuller, J. Lu, S. A. Wolf, H.-T. Kim, M. Liu, and R. D. Averitt, Ultrafast electron-lattice coupling dynamics in VO_2 and V_2O_3 thin films, Phys. Rev. B **96**, 094309 (2017).

[31] G. Lantz, B. Mansart, D. Grieger, D. Boschetto, N. Nilforoushan, E. Papalazarou, N. Moisan, L. Perfetti, V. L. R. Jacques, D. Le Bolloc'h, C. Laulhé, S. Ravy, J-P Rueff, T. E. Glover, M. P. Hertlein, Z. Hussain, S. Song, M. Chollet, M. Fabrizio, and M. Marsi, Ultrafast evolution and transient phases of a prototype out-of-equilibrium Mott-Hubbard material, Nat. Commun. **8**, 13917 (2017).

[32] M. R. Otto, L. P. René de Cotret, D. A. Valverde-Chavez, K. L. Tiwari, N. Émond, M. Chaker, D. G. Cooke, and B. J. Siwick, How optical excitation controls the structure and properties of vanadium dioxide, Proc. Natl. Acad. Sci. **116**, 450 (2019).

[33] F. Giorgianni, J. Sakai, and S. Lupi, Overcoming the thermal regime for the electric-field driven mott transition in vanadium sesquioxide, Nat. Commun. **10**, 1159 (2019).

[34] S Lupi *et al.*, A microscopic view on the mott transition in chromium-doped V_2O_3, Nat. Commun. **1**, 105 (2010).

[35] M. Sandri and M. Fabrizio, Nonequilibrium gap collapse near a first-order mott transition, Phys. Rev. B **91**, 115102 (2015).

[36] M. M. Qazilbash, A. A. Schafgans, K. S. Burch, S. J. Yun, B. G. Chae, B. J. Kim, H. T. Kim, and D. N. Basov, Electrodynamics of the vanadium oxides VO_2 and V_2O_3, Phys. Rev. B **77**, 115121 (2008).

[37] V. N. Andreev, F. A. Chudnovskii, A. V. Petrov, and E. I. Terukov, Thermal conductivity of VO_2, V_3O_5, and V_2O_3, Phys. Status Solidi (a) **48**, K153 (1978).

[38] H. V. Keer, D. L. Dickerson, H. Kuwamoto, H. L. C. Barros, and J. M. Honig, Heat capacity of pure and doped V_2O_3 single crystals, J. Solid State Chem. **19**, 95 (1976).

[39] M. J. Weber, *Handbook of Optical Materials* (CRC Press, Boca Raton, FL, 2001).

[40] C. Caddeo, C. Melis, A. Ronchi, C. Giannetti, G. Ferrini, R. Rurali, L. Colombo, and F. Banfi, Thermal boundary resistance from transient nanocalorimetry: A multiscale modeling approach, Phys. Rev. B **95**, 085306 (2017).

[41] Irving H. Malitson, Refraction and dispersion of synthetic sapphire, J. Opt. Soc. Am. **52**, 1377 (1962).

[42] G. Hamaoui, N. Horny, C. L. Gomez-Heredia, J. A. Ramirez-Rincon, J. Ordonez-Miranda, C. Champeaux, F. Dumas-Bouchiat, J. J. Alvarado-Gil, Y. Ezzahri, K. Joulain, and M. Chirtoc, Thermophysical characterisation of VO_2 thin films hysteresis and its application in thermal rectification, Sci. Rep. **9**, 8728 (2019).

[43] C. Giannetti, F. Banfi, D. Nardi, G. Ferrini, and F. Parmigiani, Ultrafast laser pulses to detect and generate fast thermomechanical transients in matter, IEEE Photonics J. **1**, 21 (2009).

[44] F. Banfi, F. Pressacco, B. Revaz, C. Giannetti, D. Nardi, G. Ferrini, and F. Parmigiani, Ab initio thermodynamics calculation of all-optical time-resolved calorimetry of nanosize systems: Evidence of nanosecond decoupling of electron and phonon temperatures, Phys. Rev. B **81**, 155426 (2010).

[45] S. Lee, K. Hippalgaonkar, F. Yang, J. Hong, C. Ko, J. Suh, K. Liu, K. Wang, J. J. Urban, X. Zhang, C. Dames, S. A. Hartnoll, O. Delaire, and J. Wu, Anomalously low electronic thermal conductivity in metallic vanadium dioxide, Science **355**, 371 (2017).